Experimental and numerical investigations of 3D-printed Onyx parts reinforced with continuous glass fibers

Daouda Nikiema, Pascale Balland, Alain Sergent

Accepted Manuscript

Cite as:

D. Nikiema, P. Balland, A. Sergent, Experimental and numerical investigations of 3D-printed Onyx parts reinforced with continuous glass fibers, Arch. Civ. Mech. Eng. 24 (2024) 50. https://doi.org/10.1007/s43452-024-00861-5.

Experimental and Numerical Investigations of 3D-Printed Onyx Parts Reinforced with Continuous Glass Fibers

Daouda Nikiema ; Pascale Balland ; Alain Sergent

Université Savoie Mont Blanc, SYMME, F-74000 Annecy, France

Corresponding author: Daouda Nikiema

Email: daouda.nikiema@univ-smb.fr; daoudanikiema94@gmail.com

Phone / Fax : +33 4 50 09 65 67 / +33 4 50 09 65 43

Abstract

The efficient modeling of 3D printed parts, especially long fiber reinforced composite parts, is a significant concern. This paper discusses finite element modeling using the embedded element technique to simulate the mechanical behavior of specimens reinforced with long glass fibers. The study considered the concentric deposition mode of the fibers, the walls, and the solid filling pattern of the printed parts as parameters. In addition, classical numerical modeling of the composites using 2D Shell elements and an analytical prediction of the Young's modulus using the rule of mixtures were implemented. The results showed that both the classical 2D Shell modeling and the law of mixtures predict the Young's modulus with acceptable prediction error. However, these approaches have limitations in predicting the overall behavior of the specimens. The use of the embedded element technique allowed for the prediction of both the Young's modulus and the global behavior of the specimens with acceptable prediction error.

Keywords: 3D Printing; Glass Fibers; Mechanical Properties; Finite Element Modeling; Embedded Elements

1 Introduction

The field of 3D printing, particularly for long or continuous fiber composites, has garnered significant interest from scientists and manufacturers. The advent of sophisticated industrial printers has contributed to the significant growth of the 3D printing market. One popular printer, manufactured by Markforged [1,2], enables the printing of parts reinforced with continuous glass, Kevlar, or carbon fibers. Dickson et al. [3] characterized the mechanical properties of the three types of fibers available in this printer and concluded that carbon fibers exhibit higher mechanical properties than the other fibers. Díaz-Rodríguez et al. [4] carried out a literature review on mechanical properties, various mechanical tests, and fractography studies of the same three types of fibers. The primary parameters for printing long fiber reinforced parts are the pattern type and matrix filling density (solid, triangular, rectangular, hexagonal, and gyroid), fiber deposition mode (concentric, isotropic, or mixed), and fiber orientation angle (e.g., 0°, 45°, or 90°). For example, Saeed et al. [5] used a solid pattern (100% density), isotropic fiber deposition mode, and orientation angles of 0°, +/-45°, and 90° in their work. Prajapati et al. [6] investigated the impact of glass fiber volume ratio on strength and found that greater fiber volumes result in higher impact resistance. Researchers are currently focused on predicting the mechanical properties and behaviors of parts printed and reinforced with long fibers using analytical and/or numerical models.

There are various analytical methods available to predict mechanical properties, such as the Rule of Mixture approach (RoM), the Classical Laminate Theory approach (CLT), and the Volume Average Stiffness (VAS) approach. Previous studies, such as Saeed et al. [5], have utilized RoM and CLT to predict the Young's modulus for carbon fiber reinforced specimens and found that both methods are effective. Lupone et al. [7] investigated all three analytical approaches for predicting elastic mechanical properties and reported a maximum error of 12.4% and 36.4% for the Young's modulus and the yield strength, respectively. However, Yu et al. [8] found that the prediction errors using VAS are high for small %volume of fiber, but for larger fiber volumes, the errors become acceptable and consistent with previous studies. For instance, Al Abadi et al. [9] reported a maximum prediction error of 7.49% for Young's modulus using the VAS method with 40% fiber volume. In contrast, Naranjo-Lozada et al. [10] found that the prediction error between RoM and tensile tests can reach 60% for a fiber volume ratio of 33%. Additionally, numerical simulation methods, such as the finite element method, can also be used to predict mechanical properties of parts.

Most numerical modeling of 3D printed composites is done using the finite element method with 2D Shell elements. Žmindák et al. [11] used 2D shell modeling in their work and found it to be effective in predicting elastic properties. Similarly, Avanzini et al. [12], Al Abadi et al. [9], and Koruche et al. [13] also used 2D shell modeling and confirmed its ability to predict elastic properties. Other authors [14] have used homogenization techniques to model the behavior of 3D printed composites. However, recent advances in modeling properties and mechanical behavior have led to the development of a new modeling technique based on embedded elements. This technique represents the fibers and matrix as separate parts that are assembled to form the composite material and has the advantage of being able to reproduce the deposition path of the fiber layers. Avanzini et al. [12] and Zhang et al. [15] have demonstrated the relevance of this technique in their work.

Despite the progress made in numerical and analytical modeling techniques, there are still certain parameters that are not considered, such as the walls of printed parts and the plasticity of the matrix. Additionally, the mechanical properties predicted by these methods are limited to the elastic domain of the parts, which restricts the ability to predict their global behavior. The main contribution of this work will be to consider the main printing parameters in the numerical simulation in order to predict the properties and mechanical behavior of 3D printed long fiber composite parts. The objective of this

study is to overcome the limitations observed in literature by considering the properties (elasticity and plasticity) of the walls and the solid pattern to predict the global behavior of printed parts. Predicting the mechanical properties of 3D-printed parts is critical as it reduces the number of physical tests essential to validate a design. In the context of 3D printing, where various printing parameters are available, anticipate the mechanical behavior of components before the printing process becomes mandatory. Otherwise, numerical prediction of mechanical properties provides several advantages, such as the potential to optimize the process. In order to achieve this goal, the work will be carried out in three parts as follows. The first section will present the experimental and numerical approach. The second section will present the results and discussions. Finally, the third section will provide the conclusion and perspectives for future work.

2 Materials and Methods

2.1 3D Printer and Materials

The printer used in the present work is the Markforged X7 industrial series commercial printer, which is capable of printing plastic parts reinforced with long fibers in a maximum volume of 330 mm x 270 mm x 200 mm. The printer is equipped with two nozzles, one for printing the plastic and the other for printing the reinforcements, and they do not operate simultaneously. It uses various plastic materials, including Onyx, Onyx FR (Flame Retardant), Onyx FR-A (Flame Retardant - Aeronautic), white Nylon, and precise PLA (Polylactic Acid) and various long fibers such as glass fibers, carbon fibers, and Kevlar fibers for reinforcement. More information on the process can be found in [7,16]. For this study, Onyx plastic and glass fibers were used. Onyx is a mixture of polyamide 6 (Nylon) and short carbon fibers, according to the manufacturer, the short carbon fiber volume is approximately 10 to 20%. The fiber lengths range from 7.035 to 44.58 µm and are mostly oriented along the printing direction [17]. A scanning electron microcospic (SEM) image, displayed in Fig. 1, depicts the main components of onyx, which are carbon microfibers and nylon. The glass fiber filament used by Markforged contains a mixture of glass fibers, nylon, and other constituents, with a volume of glass fibers at about 35%, as reported by Goh et al. [18]. The constituent parts of the glass fiber filament are shown in Fig. 2. The print setup is performed using the Eiger software from Markforged, which offers several printing parameters, including layer thickness, number of walls, roofs, and floors, type of plastic printing pattern (solid, triangular, rectangular, hexagonal, and gyroid), orientation and positioning (flat, on-edge, and vertical) on the printing platform, fiber placement mode (isotropic and concentric mode), number of fiber layers, and fiber orientation (0°, 30°, 45°, 90°, etc.).

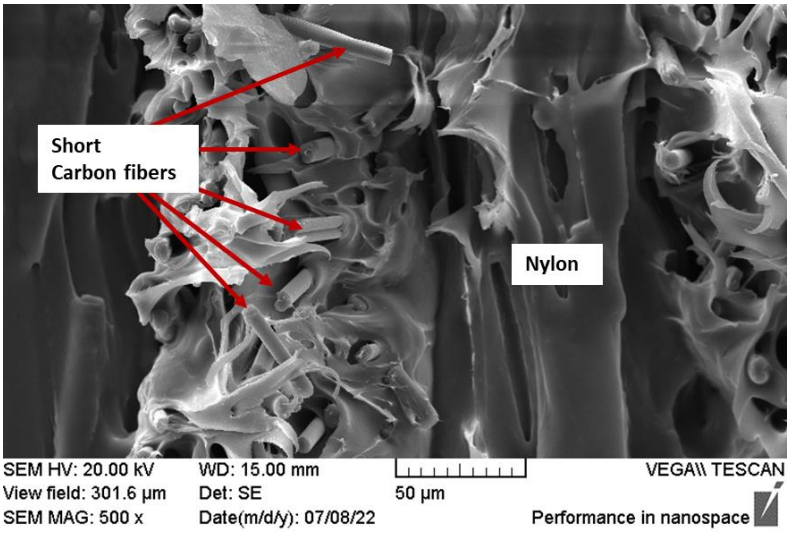

Fig. 1. Scanning electron microscopy of Onyx material.

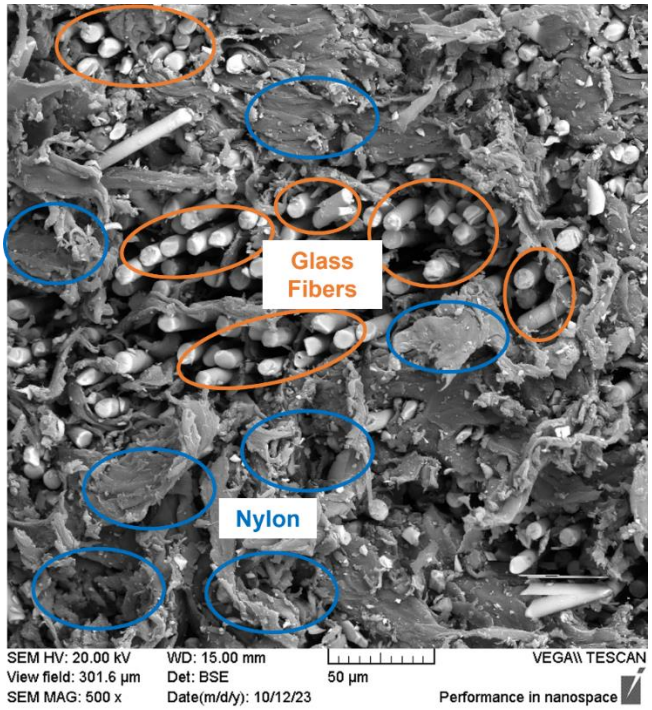

Fig. 2. 3D printed glass fibers details (scanning electron microscopy image).

2.2 Experimental Setup

In this study, uniaxial tensile tests were performed to determine the mechanical properties of the printed specimens. Firstly, the mechanical properties of the specimens printed using only Onyx were determined. In the second step, the mechanical properties of the glass fiber reinforced specimens were characterized. The tests were performed using an Instron tensile testing machine with a 50 kN force cell and an extensometer with an initial length of 12.5 mm to measure strains and stresses. The mechanical properties, such as Young's modulus and yield strength for Onyx specimens, and Young's modulus for the glass fiber reinforced specimens were determined. Three specimens were tested for each test, and the average mechanical properties were calculated.

The specimens used in the experiments were rectangular in shape, with dimensions given in Fig. 3 according to ASTM D3039. They were designed using CAD software (educational version of Inventor

software) and then imported into the Eiger software in STL (Standard Tessellation Language) format to set the printing parameters. The main printing parameters used in this study are listed in Table 1.

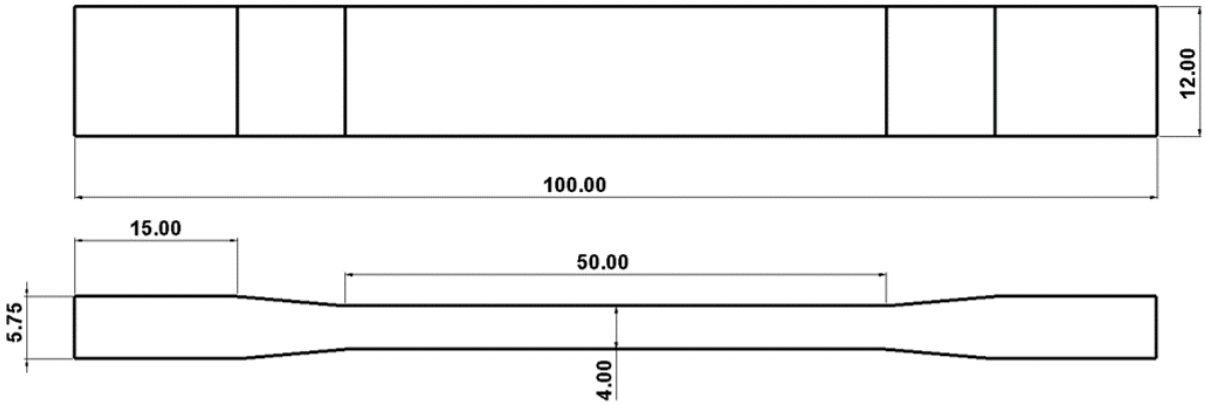

Fig. 3. Shape and dimensions (in millimeter) of the specimen.

Table 1. Printing parameters

Parameters	Specifications
Pattern and density	Solid - 100%
Layer thickness – wall width	0.1 mm – 0.4 mm
Walls (contours) count	2
Fibers deposition mode	Concentric mode
Fibers strippe count	2
Fibers layer per strippe	6
Number of concentric fibers	3 – 5

2.2.1 Onyx, Glass fiber specimens and Tensile test

To accurately predict the properties of printed parts, it is necessary to determine the elastic properties, such as Young's modulus and yield strength, of the printing materials. In this study, the elastic properties of pure Onyx and pure glass fiber specimens were determined, as well as the plasticity parameters of Onyx. To better understand the properties of the printed parts, the properties of the walls (Fig. 4b) and the solid pattern (Fig. 4c) were also characterized. This was achieved by printing a specimen with five layers of walls, which were then cut out and tested separately. Similarly, a specimen with a single wall was printed and the solid pattern was characterized by cutting out the wall. The solid pattern had a fill density of 100% and successive layers were oriented at ±45° (Fig. 4a). The main parameter analyzed in this study is Young's modulus, which was calculated by considering the linear part of the nominal stress-strain curve, as also done by S. Hasanov et al. in their work [19]. The Young's modulus was determined using Excel software and a regression coefficient of $R2 > 0.99$ over the linear part of the curves was considered. To ensure accuracy, each test was conducted using three samples under the same testing and printing conditions, taking into account the required number of tests. The power law of Hollomon, given by Eq. 1, was used to determine the plasticity parameters of Onyx samples. After the cutting operations, the dimensions of the specimens were checked to ensure that they were identical. The mechanical properties of the glass fibers (at 0°, 90°, and ±45°) were

determined from specimens with dimensions of 100 mm x 10 mm x 1.2 mm (Fig. 4d). Tests were carried out at a speed of 10 mm/min, in accordance with the recommendations of ASTM D638 and ASTM D3039.

$$\sigma = K * \varepsilon^n \quad (1)$$

Where σ, ε, and K, n refer to stress, plastic strain and intrinsic material parameters, respectively.

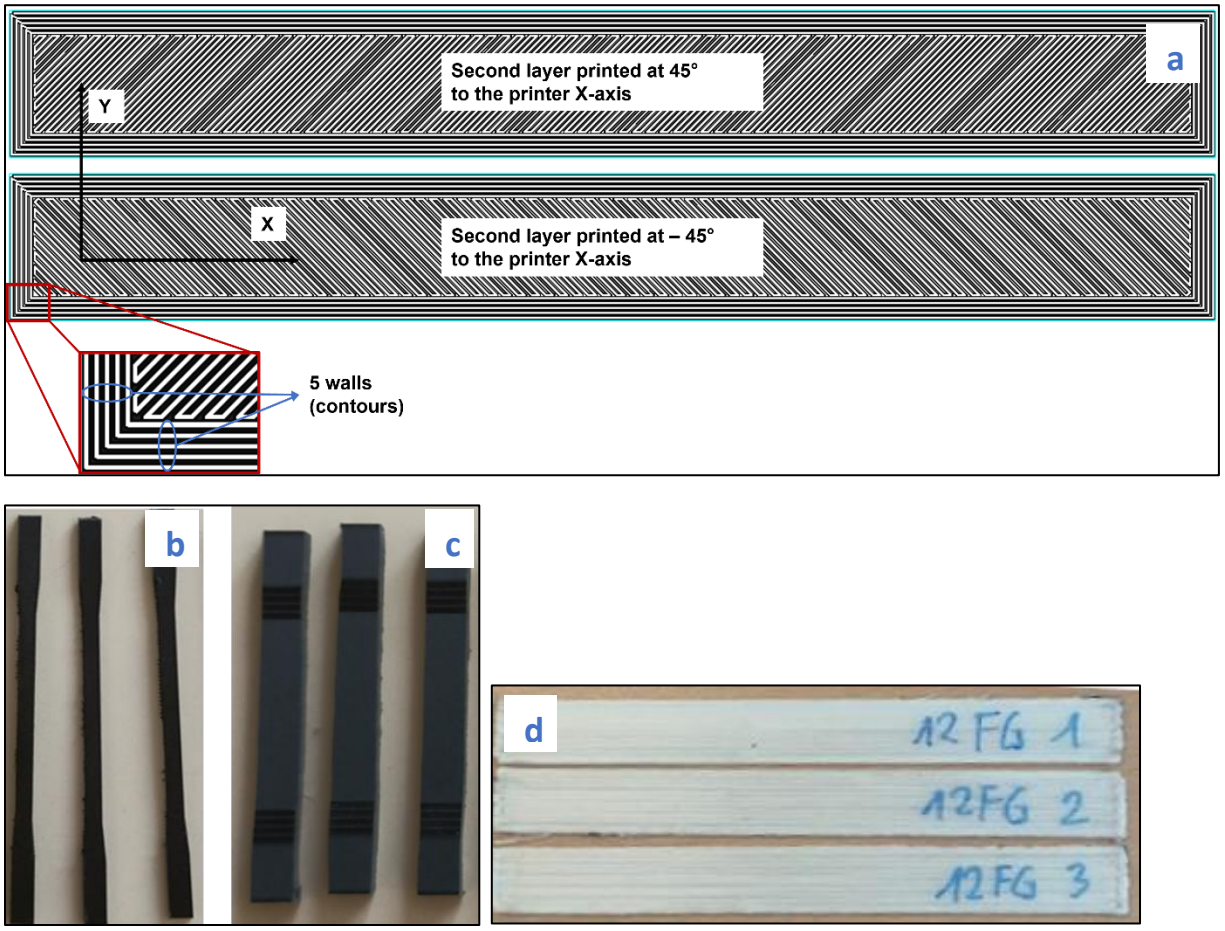

Fig. 4. Onyx and glass fiber specimens: a – layers deposition and walls illustration, b – pure wall specimens, c – pure solid specimen and d – 0° printed glass fiber.

2.2.2 Reinforced Parts and Tensile test

The glass fiber reinforced specimens were printed using the parameters listed in Table 2. The Marforged X7 printer offers two fiber deposition modes (isotropic and concentric mode), which are shown in Fig. 5. The isotropic mode allows fibers to be printed at multiple angles (Fig. 5a), while the concentric mode enables fibers to be printed by contouring around the part (Fig. 5b). In this study, only the concentric fiber deposition mode was examined. Two types of specimens with different numbers of concentric fibers were investigated, and their details are presented in Table 2. The Young's modulus of each type of specimen was determined by conducting tensile tests at a speed of 10 mm/min and following the test conditions recommended by ASTM D3039. This standard outlines the method for determining Young's modulus, which involves considering the slope of the tensile curve between 0.1% and 0.3% strain as the value for Young's modulus.

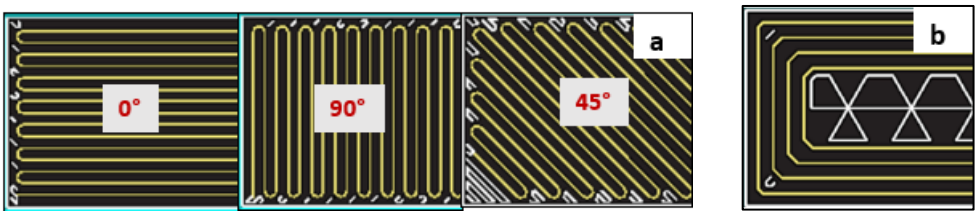

Fig. 5. Fibers Reinforcing mode: a – isotropic mode (fibers at 0°, 90° and 45°) and b – concentric mode

Table 2. Concentric mode parameters adopted of the 2 specimens studied.

	Fiber Stripe count	Fiber Layers per Stripe	Concentric Fiber count
3CF-6LS-2FS	2	6	3
5CF-6LS-2FS	2	6	5

Where CF, FS and LS refer to the count of concentric fiber, the count of fibers stripe and the number of fiber layers per stripe, respectively. Fig. 6 shows the details of **3CF-6LS-2FS** specimen.

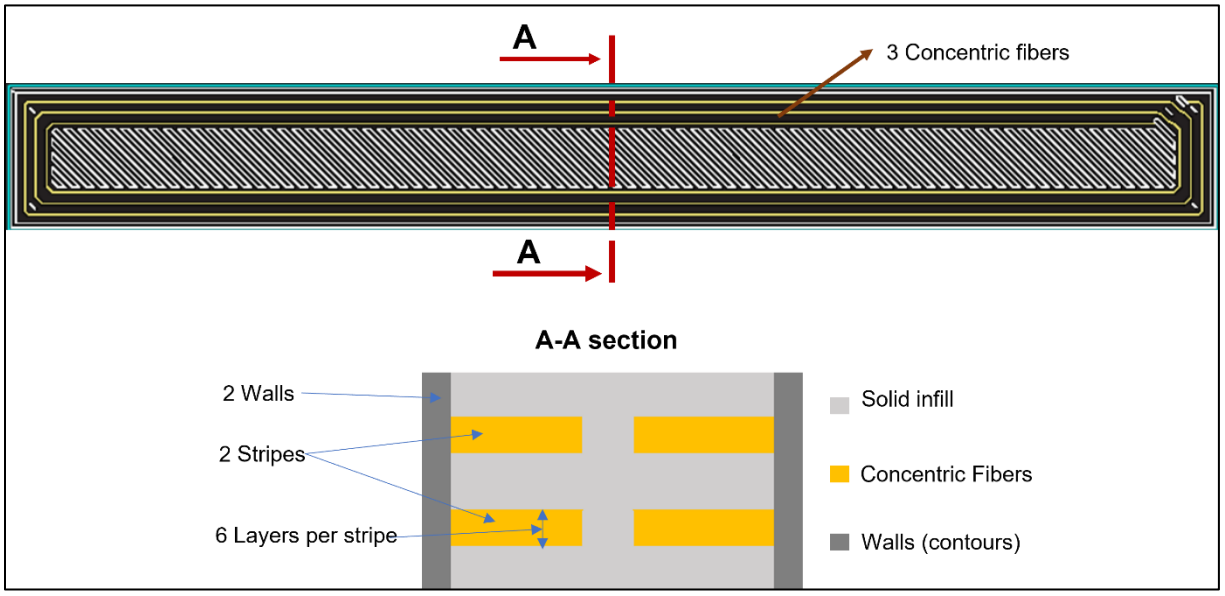

Fig. 6. Details of 3CF-6FL-2FS specimen.

2.3 Mechanical Properties Prediction with Rule of Mixture Approach

In this study, a rule of mixture (RoM) approach was used to predict the Young's modulus of the reinforced specimens. This approach considers the number of walls, fibers, and solid patterns present in the specimen. The equation used to establish the relationship between the Young's modulus and these parameters is given as Eq. 2.

$$E = v_f * E_f + v_w * E_w + v_s * E_s \quad (2)$$

Where E_f, E_w and E_s refer to the Young's modulus of Glass fiber, walls (contours) and solid pattern, respectively. v_f, v_w and v_s are volume ratio of fibers, walls and solid respectively, there are calculated by Eq. 3 to Eq. 5. The different constituents used in Eq. 2 are summarized in Table 3.

$$v_f = \frac{2*(N_{CF}*width_f*Thickness_f)*N_{FS}*N_{LS}}{A} \quad (3)$$

$$v_w = \frac{2*(N_w*width_w*Thickness_w)*Thickness_{specimen}}{A} \quad (4)$$

$$v_s = 1 - (v_w + v_f) \quad (5)$$

Table 3. Parameters used in equation 3 to 5

	Definition	**Value**
$\boldsymbol{N_{CF}}$	Number of concentric fibers	User defined
$\boldsymbol{width_f}$	Width of printed fiber	0.9 mm (fixed)
$\boldsymbol{Thickness_f}$	Thickness of printed fiber	0.1 mm in this work (fixed)
$\boldsymbol{N_{FS}}$	Number of fiber stripes	User defined
$\boldsymbol{N_{LS}}$	Number of fiber layers per stripe	User defined
$\boldsymbol{A}$	Cross section of the specimen	$48\ mm^2$ in this work
$\boldsymbol{N_w}$	Number of walls (contours)	User defined
$\boldsymbol{width_w}$	Width of wall	0.4 mm (fixed)
$\boldsymbol{Thickness_w}$	Thickness of wall	Same as $Thickness_f$ (0.1 mm)
$\boldsymbol{Thickness_{specimen}}$	Thickness of the specimen	4 mm in this work

2.4 Numerical Simulations

This study implemented two types of numerical simulations to predict the mechanical behavior and properties of the specimens based on the parameters used in the RoM approach. The first approach involved a 2D shell element model for the classical modeling of composites, while the second approach used embedded elements. Both numerical simulations were performed using Abaqus, a commercial software.

2.4.1 Classical Shell Modeling

The classical composite modeling technique which uses the theory of plies or laminates, is commonly used in the literature for simulating the mechanical behavior of 3D printed composites. Avanzini et al. [12] employed this technique and reported that the results are consistent with experimental results. Žmindák et al. [11] also used this modeling technique in their work. The approach involves treating each printed layer as a 2D shell element. The Onyx layers, including the solid pattern and walls, are considered isotropic materials, while the glass fiber layers are considered as transverse isotropic material. The material properties used for the simulation are listed in Table 5 and Table 6. Fig. 7 illustrates the numerical model of the tensile test conducted on specimen 3CF-6LS-2FS, it shows the different sections of the specimen, including the walls, fibers, and solid pattern, which were meshed with 2D elements of type S4R (Shell 4 Nodes Reduced integration) with an approximate size of 0.4 mm per element.

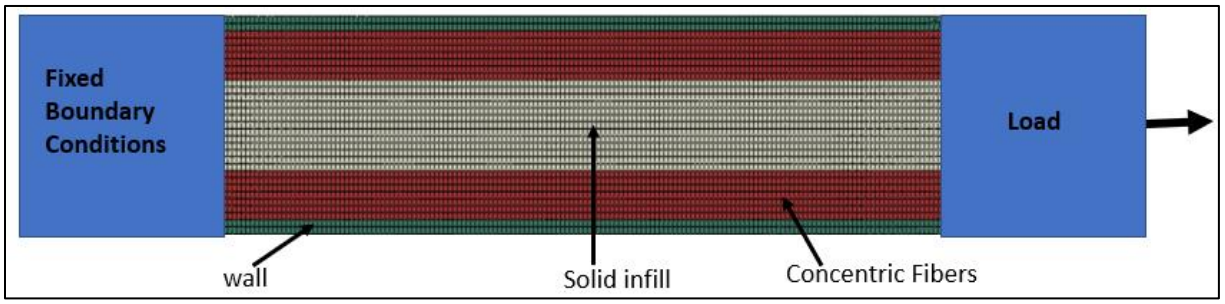

Fig. 7. Classical composite modeling of 3CF-6LS-2FS specimen (2D Shell modeling).

2.4.2 Modeling with Embedded Element Technique

The embedded element technique, commonly used in the construction industry to simulate reinforced concrete beams [20,21], has been applied in this study. This technique involves two elements: the "host" element and the "embedded" element. The "host" element is usually a solid body or volume, while the "embedded" element represents the reinforcing material, such as beams or trusses. In this study, the "host" element is Onyx, and the "embedded" element is glass fibers. The Onyx was meshed into a C3D8R (8-node brick element with reduced integration) volume element, while the fibers were meshed into a B31 (2-node beam element) 1D element, with an approximate size of 0.4 mm/element. The overall modeling approach based on embedded elements is presented in Fig. 8, and the numerical model is illustrated in Fig. 9 that shows the embedded zones.

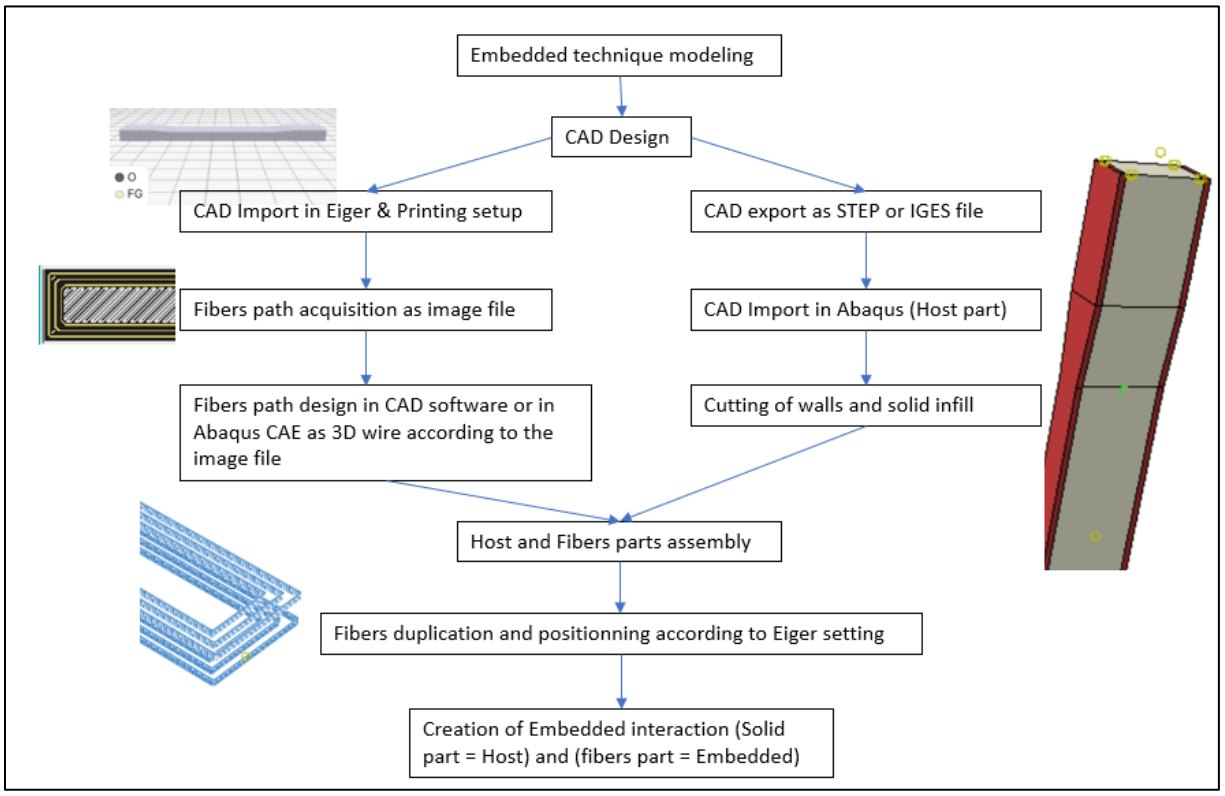

Fig. 8. Workflow of embedded element technique modeling

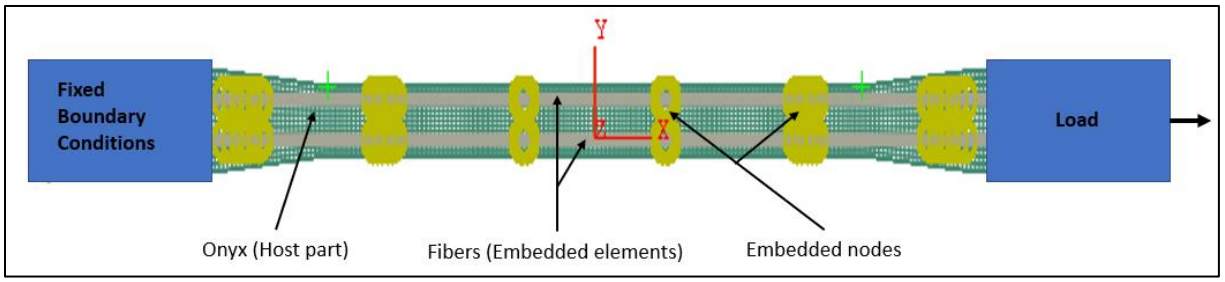

Fig. 9. Embedded model of the tensile specimen

Based on the composition of the printed glass fibers, which is a combination of Nylon and glass fibers (as shown in Fig. 2), it is possible to determine the effective Young's modulus of the glass fibers by considering the %void and the Young's modulus of the printed glass fibers (glass fibers + Nylon + void). To determine the %void, a method involving digestion of Nylon in sulfuric acid from a printed glass fiber specimen was employed in accordance with ASTM D3171. The results reveal that the printed glass fibers contain approximately 8% void, 32.96% glass fibers, and 59.05% Nylon by volume. Using this data, the effective Young's modulus of the glass fibers (E_{GFiber}) can be calculated using a relationship based on the law of mixtures (Eq. 6), which was found to be 70000 MPa, consistent with values reported in the literature for glass fibers [22].

$$E_{GFiber} = \frac{E_1 - \%Nylon * E_{Nylon}}{\%GFiber} \quad (6)$$

The printed glass fibers have a rectangular cross-section with dimensions of approximately 0.9 mm width and 0.1 mm thickness, resulting in a nominal cross-sectional area of about 0.09 mm^2. However, considering the volume ratio of 32.96% for glass fibers, we can determine the actual cross-sectional area of the glass fibers. The calculations yield an actual cross-sectional area of 0.029 mm^2 with dimensions of approximately 0.52 mm width and 0.057 mm thickness. Further details on the equations used for these calculations can be found in reference [12]. A summary of all parameters used for the modeling in this section can be found in Table 4.

Where E_1 is the Young's modulus of printed glass fiber (given in Table 6 at section 3.1.1), $\%Nylon$ is volume % of Nylon (59.05 %), E_{Nylon} is the Young's modulus of Nylon (1700 MPa according to Markoged datasheet) and $\%GFiber$ is the volume % of Glass Fiber.

Table 4. Parameters used for glass fibers modeling (Embedded element)

Parameters	Specifications
Element type	Beam (B31)
Section dimension (Width – Thickness)	0.52 mm – 0.057 mm
Young's modulus	70,000 MPa
Poisson ratio	0.25

3 Results and Discussion

This section presents the results of the experimental and numerical analysis of the tensile test. The mechanical properties of the glass fibers and Onyx (walls + solid pattern) obtained from the tensile tests are presented. Additionally, the experimental Young's modulus of the two types of glass fiber reinforced specimens is discussed. Finally, the numerical results obtained by the finite element method

using classical composite modeling with 2D Shell elements and the embedded element technique are presented, compared and analyzed.

3.1 Experimental Results

3.1.1 Onyx and Glass fiber Properties

Table 5 presents the average mechanical properties of Onyx (Walls and Solid Pattern), while Fig. 10 shows the stress-strain curve obtained from tensile test. The results indicate that the walls were mechanically stronger than the solid pattern. Specifically, the walls had a Young's modulus that is 70% higher than the solid pattern, and 57% stronger than the solid pattern at the elastic limit. However, the walls are also observed to be half as ductile as the solid pattern, with a maximum deformation of only about 15% compared to the solid pattern's maximum deformation of approximately 30%. This can be explained by the orientation of the walls in the same direction as the tensile test, whereas the solid pattern is oriented at ±45° with respect to the tensile direction of the specimen. The mechanical behavior of Onyx (walls + solid) is similar to that of a composite, where the walls represent plies oriented at 0° and the solid pattern represents plies at ±45°. The observed differences in behavior and mechanical properties between the walls and the solid pattern are fully justified in this case. The literature also has shown that short fiber composites have varying mechanical properties and behaviors depending on the orientation angle of the layers [23]. The mechanical properties obtained in this section (Table 5 and Table 6) were used in Sections 2.3 and 2.4, respectively, for predicting mechanical properties with the RoM and numerical simulations. The elastic mechanical properties (average) of the glass fibers were determined and presented in Table 6. The obtained values were found to be similar to those reported in the literature, such as those obtained by Justo et al. [24]. Interestingly, the Young's modulus of the glass fibers provided by the manufacturer was found to be 21000 MPa, which is lower than the values obtained in this study and the one obtained by Justo et al. These parameters were used in sections 2.3 and 2.4 for the RoM and numerical simulations, respectively.

Table 5. Mechanical properties (elastic and plastic parameters) of Onyx (walls and solid)

	E (MPa)	**Re (MPa)**	**Hollomon plasticity parameters (K ; n)**
Walls	5530±340	54±5	142.5 ; 0.142
Solid	1660±150	24±2	63.63 ; 0.148

Table 6. Elastic properties of printed glass fibers

	E_1 **(MPa)**	E_2 **(MPa)**	ν_{12}	G_{12} **(MPa)**
Test values	24095±1240	810±8.16	-	1126±334
Justo et al. [24]	25860	1130	0.37	880

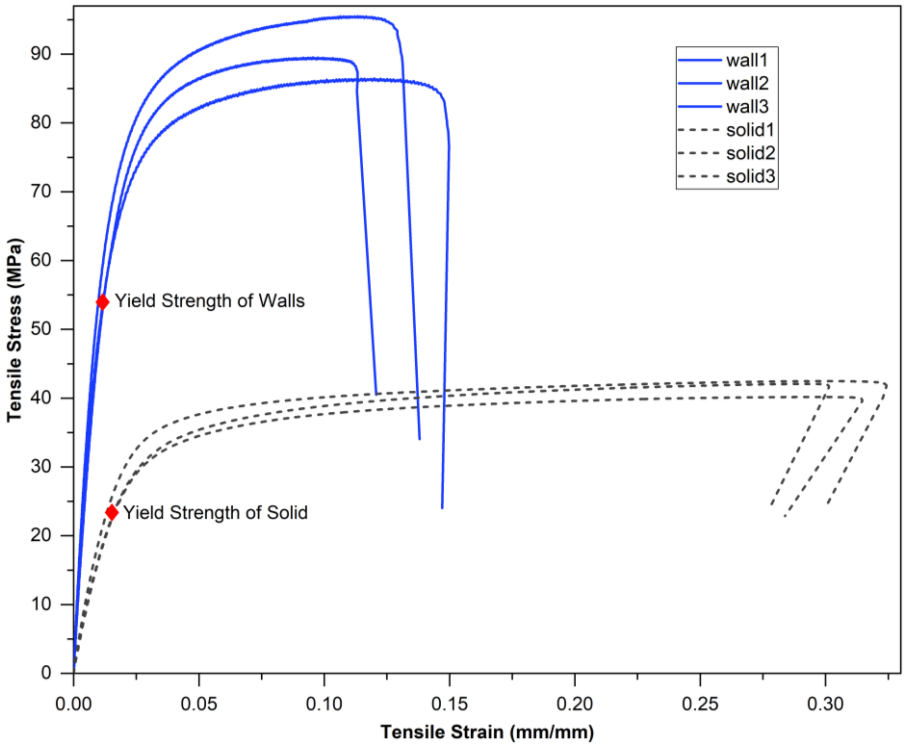

Fig. 10. Tensile stress-strain curves of Onyx (walls and solid infill)

3.1.2 Reinforced Parts Properties

Table 7 and Fig. 11 present the Young's modulus and tensile curves, respectively, for the two types of specimens studied (**3CF-6LS-2FS** and **5CF-6LS-2FS**). The results indicated that the **5CF-6LS-2FS** specimen was stiffer and stronger than the **3CF-6LS-2FS** specimen, which is expected due to the higher fiber volume in the specimen. The mechanical behavior curves revealed that most of the plasticity of Onyx is absorbed by the glass fibers, resulting in low plasticity. Moreover, the curves demonstrated that the **3CF-6LS-2FS** specimen undergoes more deformation than the **5CF-6LS-2FS** specimen (3% and 4% deformation, respectively). These findings are consistent with those reported by Melenka et al. [25] and Yu et al. [8]

Table 7. Young's modulus of reinforced specimens

	3CF-6LS-2FS	**5CF-6LS-2FS**
Young's modulus E (MPa)	5438±264	8183±269

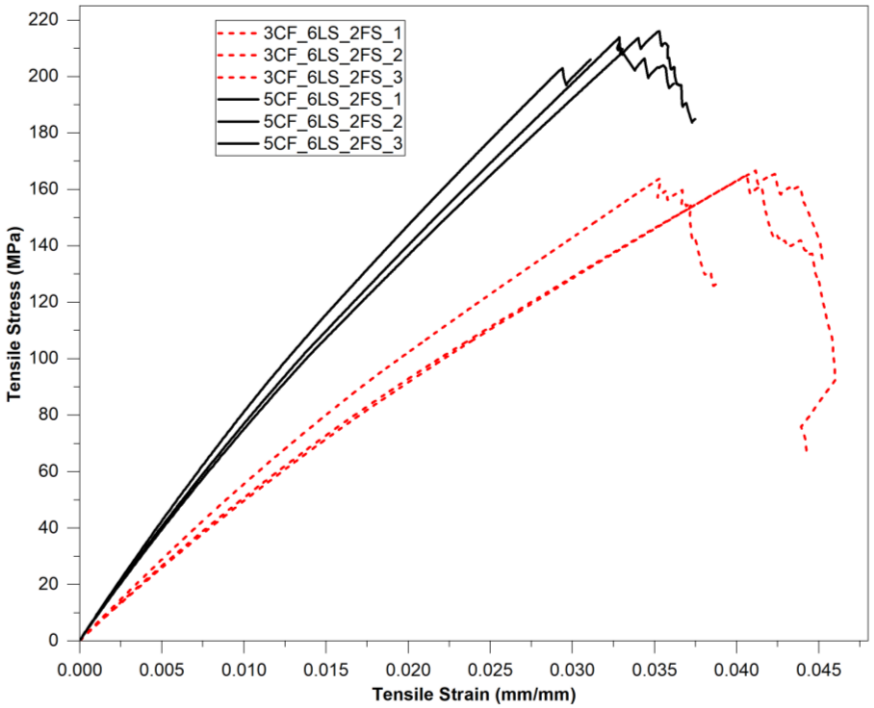

Fig. 11. Tensile stress-strain curve of specimens: 3CF-6LS-2FS and 5CF-6LS-2FS specimens

3.2 Rule of Mixture Results

The RoM is an analytical method used to determine the elastic properties of composite materials quickly. This approach was applied in the present study, and the results are presented in Table 8 and discussed in this section. The method provides volume ratios of the constituents (walls, solid, and fibers) and the values of Young's moduli of the two specimens. The volume ratios of the constituents were calculated using Equations 3 through 5, and the Young's modulus was obtained using Equation 2. The fiber volume fractions of the two specimens were 13.5% and 22.5%, respectively, resulting in Young's moduli of 5174 MPa and 7185 MPa, which were very close to the experimental values. This indicates that the method was quite effective in predicting the mechanical properties of glass fiber reinforced parts with a high fiber volume fraction. However, Díaz-Rodríguez et al. [4] showed that the mechanical properties was underestimated for specimens with fiber volume fractions exceeding 15%. Furthermore, Naranjo-Lozada et al. [10] demonstrated that for a fiber volume of 33%, the prediction compared the experimental test reached 60%. The accurate prediction of the mixture law in this study is likely due to the precise estimation of the volume fractions of the constituents and the inclusion of walls in the formulation of rule of mixture.

Table 8. Results predicted by RoM

	Fibers fraction v_f	**Walls fraction v_w**	**Solid fraction v_s**	**E (MPa)**
3CF-6LS-2FS	0.135	0.133	0.732	5174
5CF-6LS-2FS	0.225	0.133	0.642	7185

3.3 Numerical Results

3.3.1 2D Shell Modeling

The elastic properties of the **3CF-6LS-2FS** and **5CF-6LS-2FS** specimens were determined using numerical simulation with classical 2D Shell modeling. The obtained Young's moduli were 5351 MPa and 7127 MPa, respectively, which were in good agreement with the RoM results. The stress distribution of the

different parts of the specimens was also analyzed, and it was found that the stress levels of the walls and solid exceeded the experimental values obtained in Section 3.1.1. Similarly, the stress level of the glass fibers also exceeded the yield strength provided by the manufacturer. However, for considering only the elastic properties, the classical 2D Shell modeling was effective This was consistent with the findings of Žmindák et al. [11] and Avanzini et al. [12] who also confirmed the good prediction of 2D Shell elements in predicting the Young's modulus. Fig. 12 shows the stress map for ply-1 (the walls and the solid infill) and ply-6 (the fibers and the solid infill) of the specimens.

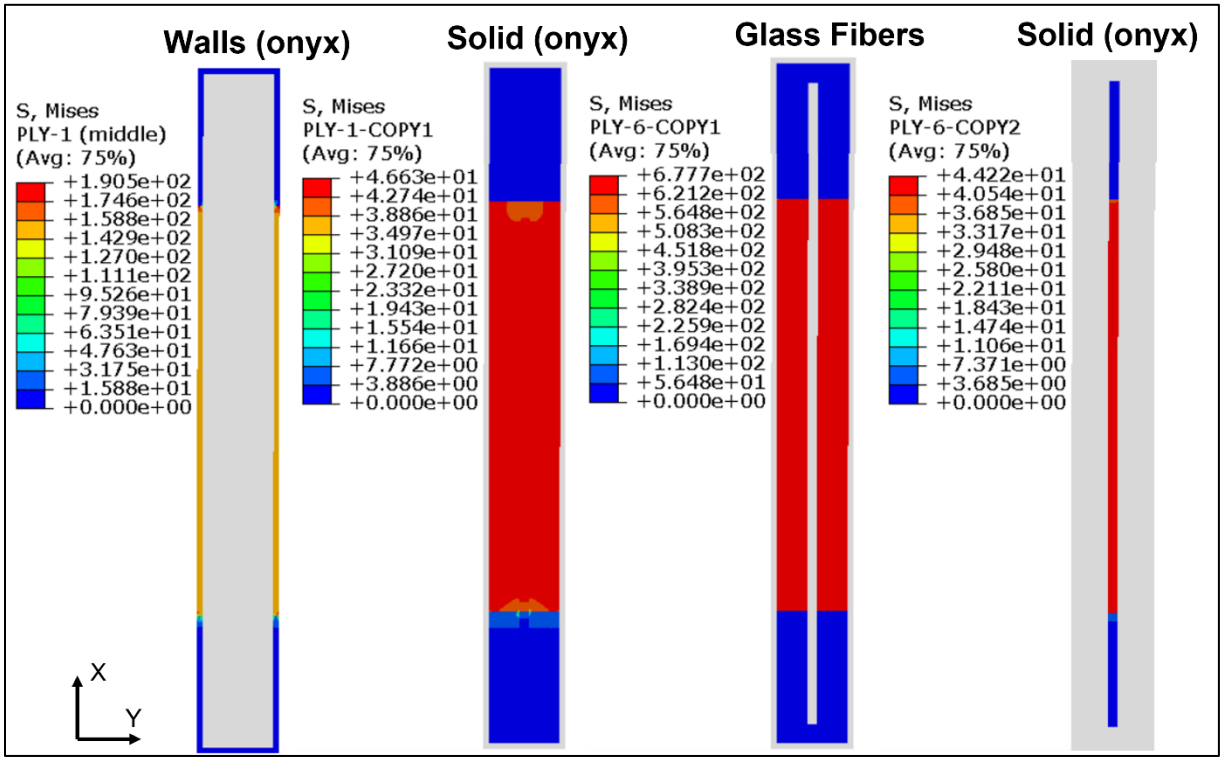

Fig. 12. Von Mises stress map obtained by classical composite simulation with 2D Shell elements. From left to right respectively the wall stresses (ply-1), the solid stresses (ply-1), the fiber stresses (ply-6) and the stresses of the solid located between the concentric fiber layers (ply-6).

3.3.2 Embedded Element Modeling

The results obtained from the numerical modeling using the embedded element technique showed the Young's modulus of 5264 MPa and 7283 MPa for the **3CF-6LS-2FS** and **5CF-6LS-2FS** specimens, respectively. These results were consistent with the results from the tensile tests, RoM, and 2D Shell modeling. The stress-strain curves of the two specimens showed that the experimental and numerical curves were similar and exhibited the same trends, indicating a good prediction of the elastic or elasto-plastic mechanical behavior of the specimens. The Von Mises stress map presented in Fig. 13 demonstrated that the maximum stress levels of the walls and Onyx accurately reproduced plasticity. The stress level reached by the fibers also demonstrated good consistency with the simulation. This technique based on embedded elements was shown to have good predictive ability in studies conducted by Avanzini et al. [12] and H. Zhang et al. [15]. The advantage of this technique is that it enables accurate reproduction of the fiber path, which is particularly important when the printed parts have complex geometrical shapes.

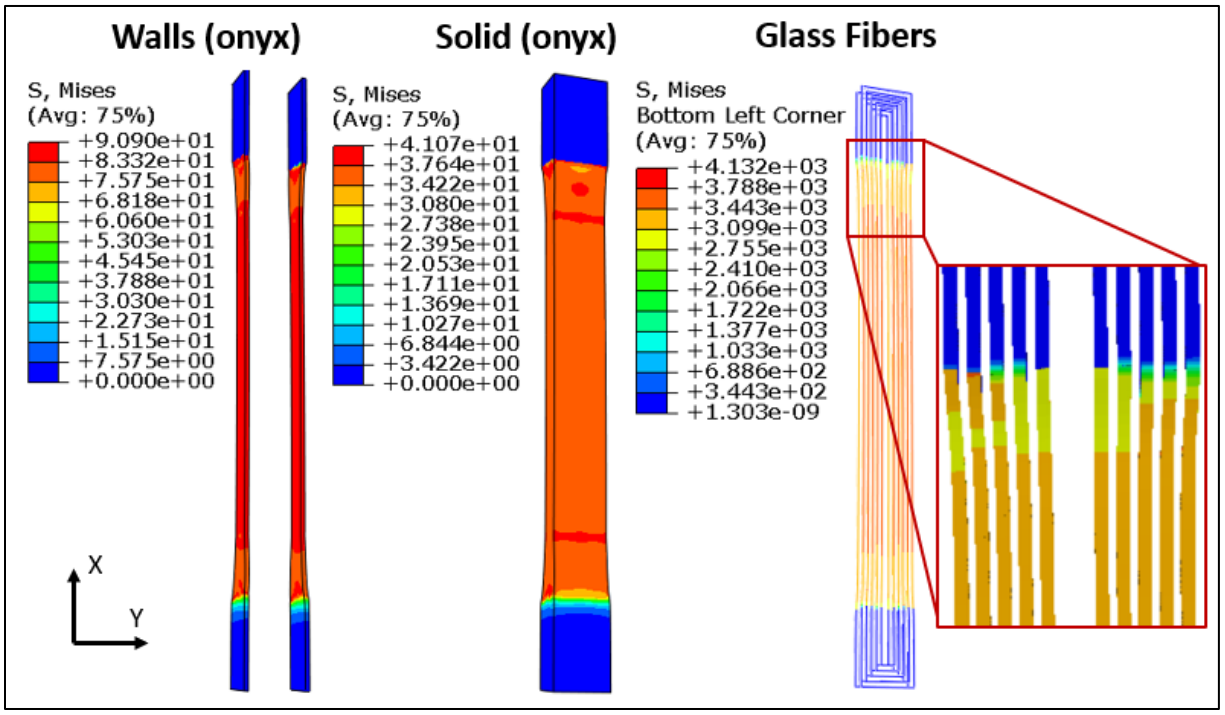

*Fig. 13. Von Mises stress map obtained by embedded element technique. From left to right respectively the wall stresses, the solid stresses, the concentric fibers stresses. Case of **5CF-6LS-2FS** specimen.*

3.4 Discussion

The results obtained from both finite element modeling and mixture law methods agreed with the experimental tests, with acceptable prediction errors compared to literature values. Table 9 shows a comparison of Young's moduli and prediction errors for the **3CF-6LS-2FS** and **5CF-6LS-2FS** samples, which are low for the former and high for the latter. This discrepancy can be attributed to the high fiber volume ratio of the **5CF-6LS-2FS** specimen (22.5% fiber volume fraction) compared to the **3CF-6LS-2FS** specimen (12.5% fiber volume fraction).

Table 9. Comparison of Young's modulus and prediction errors. Young's modulus values are given in MPa

	Test	RoM	Error (%)	Shell	Error (%)	Embedded	Error (%)
3CF-6LS-2FS	5437±264	5174	4.8	5351	1.6	5264	3.2
5CF-6LS-2FS	8182±330	7185	12.2	7127	12.9	7283	10.9

The stress-strain curves depicted in Fig.14 (a-b) demonstrate the effective prediction of the mechanical behavior by both numerical modeling methods. While the 2D Shell method accurately predicts the linear behavior, it fails to capture the global mechanical behavior, including the plasticity zone. On the other hand, the method based on embedded elements successfully predicts the overall behavior of the specimens, as it considers the plasticity of the walls and the solid pattern. The separate consideration of the walls and the pattern offers the potential for optimal design of the parts in the future.

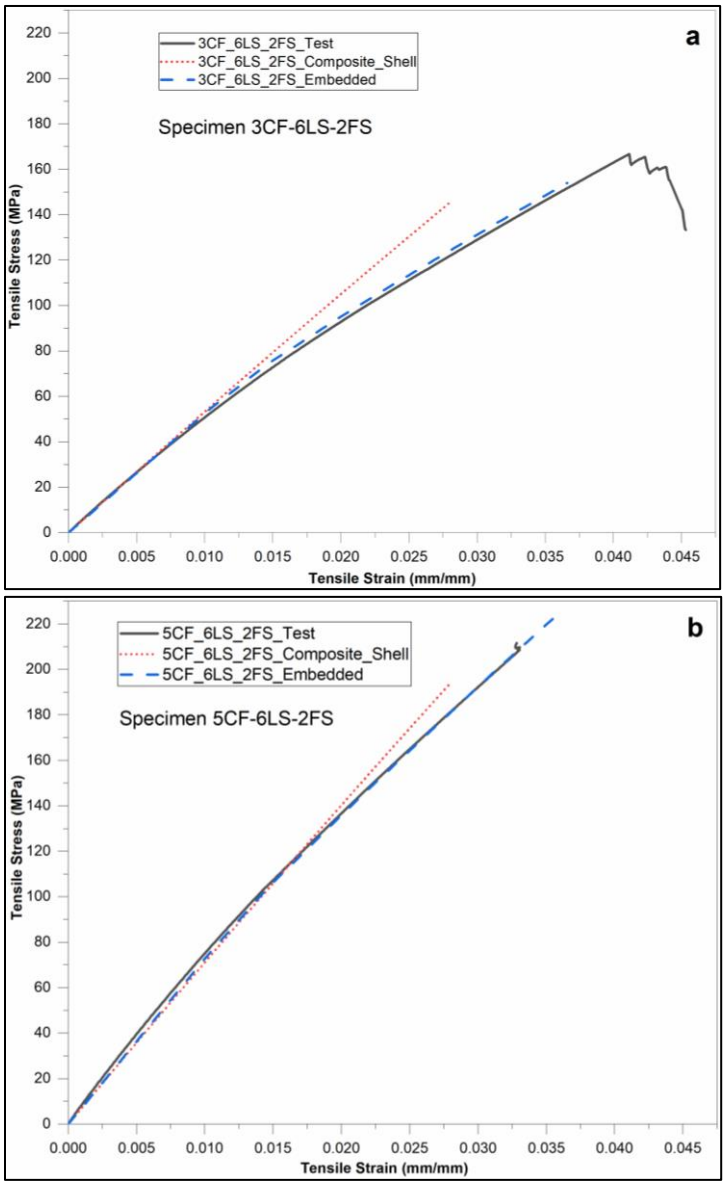

Fig. 14. Comparison of mechanical behavior of specimen. a- 3CF-6LS-2FS specimen and b-5CF-6LS-2FS specimen.

The failure analysis of the tested specimens revealed that the failure zones corresponded to the regions with the highest stresses. However, the accuracy of failure prediction could be further improved by incorporating the damage or failure modes into the numerical simulation using the embedded element technique. To predict the failure of the specimen, a ply damage criterion can be integrated into the 2D Shell simulation. X-ray tomographic observation of the cross-section of a specimen after the tensile test (Fig.15) revealed several damage phenomena:

- inter-layer delamination of glass fibers caused by weak inter-laminar adhesion between the printed fiber layers. The weak inter-laminar adhesion is due to the formation of voids between the fiber layers during printing as reported in [7] and in [15].
- Delamination between the glass fibers and Onyx was also observed due to poor adhesion at the contact surface between the two materials, which can be attributed to the difference in temperature during printing.

- Additionally, delamination between the Onyx layers was observed, which indicates poor adhesion between the printed layers.
- The section also exhibited swelling of the Onyx and glass fiber layers, probably due to the presence of porosity and poor adhesion, which facilitated some slippage of the fibers or the matrix (Onyx).

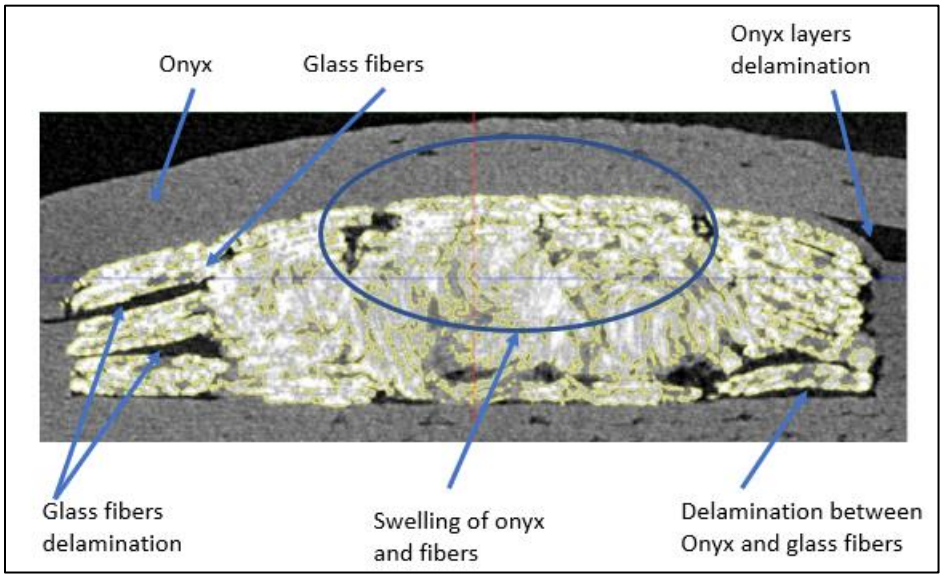

Fig. 15. X-ray tomography of reinforced specimen after tensile test.

Conventional modeling methods such as 2D Shell element modeling may face difficulty or even impossibility in accurately modeling geometrically complex parts and complex fiber paths. However, the embedded element technique has proven to be effective in accurately modeling the fiber path and representing it in numerical simulations. With this technique, the state of stresses in both the matrix (Onyx) and fibers can be determined.

The embedded element technique, despite its effectiveness, has some limitations that should be considered. One of the limitations is the added mass and stiffness of the model due to the use of embedded elements, which may affect the overall accuracy of the simulation (in fatigue or dynamic simulation). Additionally, the interface between the fibers and matrix cannot be accurately modeled using contact or cohesive elements. Finally, the embedded element technique is only applicable to host elements that do not have a rotational degree of freedom, such as C3D8R volume elements.

4 Conclusion

This study focused on investigating the mechanical properties of specimens reinforced with continuous glass fibers which included an experimental tensile test, prediction using the law of mixtures, and two numerical modeling approaches based on classical 2D Shell composite modeling and the embedded element technique. The following main conclusions were drawn from this study:

- The experimental tensile tests confirmed that the mechanical behavior, particularly the Young's modulus, was dependent on the volume of fibers contained in the specimens. The 5CF-6LS-2FS specimen, which had 9% more glass fibers by volume than the 3CF-6LS-2FS specimen, showed a Young's modulus approximately 35% higher. The stress-strain curves of both

specimens showed bilinearity in contrast to Onyx, which exhibited a distinct elastic and plastic domain, and glass fibers, which exhibited a linear elastic domain.

- The prediction of the Young's modulus using the law of mixtures yielded satisfactory results, with prediction errors between 4.8% and 12.2% compared to the experimental tensile test for the two specimens, which were relatively small errors compared to other prediction errors found in the literature.
- Both numerical simulation methods displayed acceptable prediction errors ranging from 1.6% to 12.9% and 3.2% to 10.9% for classical 2D Shell composite modeling and the embedded element technique, respectively. The use of the embedded element technique allowed for a more accurate representation of the global behavior of the two studied specimens than the classical modeling of composites with 2D Shell elements, which only had a linear elastic behavior and did not accurately reproduce the real behavior of the specimens.
- The separate characterization of the walls and the solid pattern was useful, as the results showed that they had different mechanical behaviors and properties. The walls were mechanically stronger than the solid pattern, and their consideration allowed for a more realistic and accurate numerical simulation of the mechanical behavior of the specimens.

The investigations carried out in this study pave the way for future research focusing on numerical modeling of specimens with isotropic and mixed modes of fiber deposition (concentric + isotropic). The separate consideration of walls and the solid pattern in both the prediction with the law of mixtures and the numerical simulation can lead to the development of an approach for predicting mechanical properties and behavior according to the number of walls and fibers. This could serve as a tool for optimizing printing parameters and mechanical properties of 3D printed parts reinforced with continuous fibers. Another area of future research is the consolidation of printed parts to reduce porosity and improve fiber-matrix adhesion, inter-layer adhesion of fibers, and inter-layer adhesion of Onyx.

Declarations:

Funding: This study was not funded by any funding source or organization.

Conflict of interest: The authors declare no conflicts of interest. We declare no commercial or associative interests that represent conflicts of interest in connection with this work or that could have influenced the work reported in this study

Ethical approval: This article does not contain any studies with human participants or animals performed by any of the authors.

References

[1] J. Galos, Y. Hu, A.R. Ravindran, R.B. Ladani, A.P. Mouritz, Electrical properties of 3D printed continuous carbon fibre composites made using the FDM process, Compos. Part A Appl. Sci. Manuf. 151 (2021). https://doi.org/10.1016/j.compositesa.2021.106661.

[2] Y. Zhang, C. Purssell, K. Mao, S. Leigh, A physical investigation of wear and thermal characteristics of 3D printed nylon spur gears, Tribol. Int. 141 (2020). https://doi.org/10.1016/j.triboint.2019.105953.

[3] A.N. Dickson, J.N. Barry, K.A. McDonnell, D.P. Dowling, Fabrication of continuous carbon, glass

and Kevlar fibre reinforced polymer composites using additive manufacturing, Addit. Manuf. 16 (2017) 146–152. https://doi.org/10.1016/j.addma.2017.06.004.

[4] J.G. Díaz-Rodríguez, A.D. Pertúz-Comas, O.A. González-Estrada, Mechanical properties for long fibre reinforced fused deposition manufactured composites, Compos. Part B Eng. 211 (2021). https://doi.org/10.1016/j.compositesb.2021.108657.

[5] K. Saeed, A. McIlhagger, E. Harkin-Jones, J. Kelly, E. Archer, Predication of the in-plane mechanical properties of continuous carbon fibre reinforced 3D printed polymer composites using classical laminated-plate theory, Compos. Struct. 259 (2021). https://doi.org/10.1016/j.compstruct.2020.113226.

[6] A.R. Prajapati, H.K. Dave, H.K. Raval, Effect of fiber volume fraction on the impact strength of fiber reinforced polymer composites made by FDM process, Mater. Today Proc. 44 (2021) 2102–2106. https://doi.org/10.1016/j.matpr.2020.12.262.

[7] F. Lupone, E. Padovano, C. Venezia, C. Badini, Experimental Characterization and Modeling of 3D Printed Continuous Carbon Fibers Composites with Different Fiber Orientation Produced by FFF Process, Polymers (Basel). 14 (2022). https://doi.org/10.3390/polym14030426.

[8] T. Yu, Z. Zhang, S. Song, Y. Bai, D. Wu, Tensile and flexural behaviors of additively manufactured continuous carbon fiber-reinforced polymer composites, Compos. Struct. 225 (2019) 111147. https://doi.org/10.1016/j.compstruct.2019.111147.

[9] H. Al Abadi, H.T. Thai, V. Paton-Cole, V.I. Patel, Elastic properties of 3D printed fibre-reinforced structures, Compos. Struct. 193 (2018) 8–18. https://doi.org/10.1016/j.compstruct.2018.03.051.

[10] J. Naranjo-Lozada, H. Ahuett-Garza, P. Orta-Castañón, W.M.H. Verbeeten, D. Sáiz-González, Tensile properties and failure behavior of chopped and continuous carbon fiber composites produced by additive manufacturing, Addit. Manuf. 26 (2019) 227–241. https://doi.org/10.1016/j.addma.2018.12.020.

[11] M. Žmindák, P. Novák, J. Soukup, D. Milosavljevic, M. Kaco, Finite element simulation of tensile test of composite materials manufactured by 3D printing, IOP Conf. Ser. Mater. Sci. Eng. 776 (2020). https://doi.org/10.1088/1757-899X/776/1/012082.

[12] A. Avanzini, D. Battini, L. Giorleo, Finite element modelling of 3D printed continuous carbon fiber composites: Embedded elements technique and experimental validation, Compos. Struct. 292 (2022). https://doi.org/10.1016/j.compstruct.2022.115631.

[13] U.S. Koruche, S.F. Patil, Application of Classical Lamination Theory and Analytical Modeling of Laminates, Int. Res. J. Eng. Technol. (2015) 2395–56.

[14] M. Kalova, S. Rusnakova, D. Krzikalla, J. Mesicek, R. Tomasek, A. Podeprelova, J. Rosicky, M. Pagac, 3d printed hollow off-axis profiles based on carbon fiber-reinforced polymers: Mechanical testing and finite element method analysis, Polymers (Basel). 13 (2021). https://doi.org/10.3390/polym13172949.

[15] H. Zhang, S. Wang, K. Zhang, J. Wu, A. Li, J. Liu, D. Yang, 3D printing of continuous carbon fibre reinforced polymer composites with optimised structural topology and fibre orientation, Compos. Struct. (2023) 116914. https://doi.org/10.1016/j.compstruct.2023.116914.

[16] A. Todoroki, T. Oasada, Y. Mizutani, Y. Suzuki, M. Ueda, R. Matsuzaki, Y. Hirano, Tensile property evaluations of 3D printed continuous carbon fiber reinforced thermoplastic composites, Adv. Compos. Mater. 29 (2020) 147–162. https://doi.org/10.1080/09243046.2019.1650323.

[17] D.R. Hetrick, S.H.R. Sanei, C.E. Bakis, O. Ashour, Evaluating the effect of variable fiber content on mechanical properties of additively manufactured continuous carbon fiber composites, J. Reinf. Plast. Compos. 40 (2021) 365–377. https://doi.org/10.1177/0731684420963217.

[18] G.D. Goh, V. Dikshit, A.P. Nagalingam, G.L. Goh, S. Agarwala, S.L. Sing, J. Wei, W.Y. Yeong, Characterization of mechanical properties and fracture mode of additively manufactured carbon fiber and glass fiber reinforced thermoplastics, Mater. Des. 137 (2018) 79–89. https://doi.org/10.1016/j.matdes.2017.10.021.

[19] S. Hasanov, A. Gupta, A. Nasirov, I. Fidan, Mechanical characterization of functionally graded materials produced by the fused filament fabrication process, J. Manuf. Process. 58 (2020) 923–935. https://doi.org/10.1016/j.jmapro.2020.09.011.

[20] Hamid Sinaei, Evaluation of reinforced concrete beam behaviour using finite element analysis by ABAQUS, Sci. Res. Essays. 7 (2012). https://doi.org/10.5897/sre11.1393.

[21] P. Qian, Q. Xu, Development of Embedded Element Technique for Permeability Analysis of Cracked Porous Media, Math. Probl. Eng. 2017 (2017). https://doi.org/10.1155/2017/6713452.

[22] M.S. El-Wazery, M.I. El-Elamy, S.H. Zoalfakar, Mechanical Properties of Glass Fiber Reinforced Polyester Composites, Int. J. Appl. Sci. Eng. 14 (2017) 121. https://doi.org/10.6703/IJASE.2017.14(3).121.

[23] S. Bhandari, R.A. Lopez-Anido, L. Wang, D.J. Gardner, Elasto-Plastic Finite Element Modeling of Short Carbon Fiber Reinforced 3D Printed Acrylonitrile Butadiene Styrene Composites, Jom. 72 (2020) 475–484. https://doi.org/10.1007/s11837-019-03895-w.

[24] J. Justo, L. Távara, L. García-Guzmán, F. París, Characterization of 3D printed long fibre reinforced composites, Compos. Struct. 185 (2018) 537–548. https://doi.org/10.1016/j.compstruct.2017.11.052.

[25] G.W. Melenka, B.K.O. Cheung, J.S. Schofield, M.R. Dawson, J.P. Carey, Evaluation and prediction of the tensile properties of continuous fiber-reinforced 3D printed structures, Compos. Struct. 153 (2016) 866–875. https://doi.org/10.1016/j.compstruct.2016.07.018.